Experimental Results Using Active Control of Traveling Wave Power Flow

David W. Miller and Steven R. Hall
Massachusetts Institute of Technology, Cambridge, Massachusetts 02139

This paper describes a series of active structural control experiments on a 24-ft pinned-free beam. The feedback compensators are derived using a traveling wave approach. A compensator is derived that absorbs all impinging power and therefore eliminates resonant behavior. Since this compensator is noncausal, however, a causal solution is derived using a Wiener-Hopf technique. This solution mimics the noncausal compensator in a select frequency range. The Wiener-Hopf compensator was implemented and tested experimentally, as was a simple rate feedback compensator. The performance of the optimal Wiener-Hopf compensator, as measured by the damping of the structure, far exceeds that obtainable using rate feedback.

Introduction

MANY envisioned large space structures are composed of structural elements that may be modeled as one-dimensional waveguides. Truss beams, solar panels, and antenna booms are examples of long, slender, one-dimensional members. These members exhibit wave behavior with significant propagation delays as disturbances propagate across their length. This suggests the use of a wave description to model the dynamics of such structures.[1-3]

Several researchers have approached the problem of designing wave model based controllers for elastic structures.[4-14] One approach is to absorb as much of the wave traveling toward the actuator as possible. Another approach is to shunt the energy away from sensitive locations to areas where it can be dissipated. In either case, only the local reflection and transmission behavior around the sensor/actuator pair needs to be modeled.

Local models are more appropriate than global models for certain applications. For complex structures, modal models can become numerically cumbersome and inaccurate for higher frequency modes. A local wave model can accurately capture the "dereverberated" impedance in the neighborhood of the controller even though global characteristics, such as resonant frequencies and mode shapes, are not modeled. "Dereverberated" refers to the impedance that would be revealed if the energy departing the junction never returned. The reverberant (returning) field determines the resonant characteristics. Since resonant information is not required to model the local power flow properties, it is not included in the wave model. Hagedorn and Schmidt[4] argued that wave descriptions are less sensitive and, therefore, more robust than global models of structures. Therefore, if control objectives are posed in terms of local behavior, local models may be most appropriate.

Von Flotow[2,6] and von Flotow and Schafer[5,7] first suggested a framework for the modeling of wave behavior in structures for control purposes. In this framework (Fig. 1), the structure is composed of one-dimensional waveguides (structural members) interconnected at junctions (boundaries). The waveguides carry waves that travel both toward the junction (incoming waves) and away from the junction (outgoing waves). Each junction may also have sensors and actuators for use in controlling the structure. For example, a junction may be a single member end condition, an intersection of several members, or an arbitrary location on a uniform member where control hardware is located. The basic objective of wave control is to actively alter the wave scattering properties of a junction. Junction control has obvious application where vibration suppression and dynamic isolation are required.

Much of the work in this field deals with specific examples of waveguides and lacks general applicability. For example, some methods cannot handle evanescent behavior, the spa-

David W. Miller received his S.B., S.M., and Sc.D. degrees from the Massachusetts Institute of Technology, Department of Aeronautics and Astronautics, in 1982, 1985, and 1988, respectively. Currently, he is a Research Associate in the Space Engineering Research Center at M.I.T. Research interests include active control of flexible structures, control-structure optimization, passive structural design, and pointing control. He is a member of AIAA.

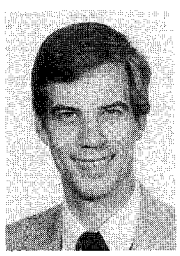

Steven R. Hall received his S.B., S.M., and Sc.D. degrees from the Massachusetts Institute of Technology, Department of Aeronautics and Astronautics, in 1980, 1982, and 1985, respectively. He is currently the Finmeccanica Career Development Assistant Professor of Engineering in the Department of Aeronautics and Astronautics at M.I.T. His research interests include active control of flexible structures, control of helicopter and machinery vibration, and control of flight vehicles. He is a member of AIAA, the Institute of Electrical and Electronic Engineers, and the American Helicopter Society.

Received Sept. 27, 1989; revision received April 4, 1990.

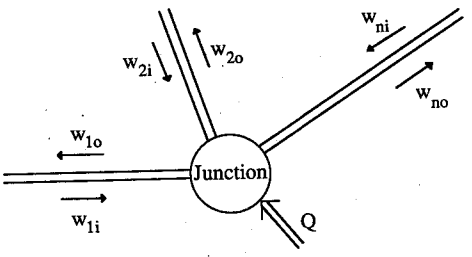

Fig. 1 Generic wave junction.

tially exponential deformation patterns that are localized about structural discontinuities and forcing locations (i.e., the hyperbolic terms in standing mode shapes). Often, feedback compensator formulations lack the required causality and stability constraints. As a result, there is an apparent need for a model-based, broadband control formulation for generic junctions that minimizes a realistic performance metric, such as net power flow through the junction. This model-based description of power flow should incorporate explicit contributions from both propagating and evanescent behavior. This complete description of power flow can provide an important means for determining closed-loop stability. Finally, the formulation should provide a constraint that the derived feedback compensator be causal and, therefore, implementable.

Miller and von Flotow[1] have pursued an approach based on explicit frequency domain descriptions of power flow due to both propagating and evanescent waves. Minimization of junction power flow corresponds to matching the junction's impedance as closely as possible given the available control degrees of freedom. Achievable performance increases as more distinct actuators and sensors are used at the junction. If the impedance is matched, modes that depend entirely on energy traversing the controlled junction will cease to exist. Originally, this power flow description, and associated member and junction dynamics, was formulated for a generic junction in order to broaden the description's applicability to complex junctions. A formulation of control compensators that minimizes junction power flow was obtained.[8] However, this formulation lacked a constraint that the compensator be causal and, therefore, implementable. This causality constraint was incorporated through both a Wiener-Hopf and a causal fixed-form parameter optimization technique.[9] Because only a local model is used, the method of Miller et al.[9] does not guarantee closed-loop stability. To insure closed-loop stability, Miller et al.[9] suggested approximating the Wiener-Hopf solution by a positive real transfer function. Although this approach is somewhat ad hoc, it has led to satisfactory compensators.

A different approach suggested by MacMartin and Hall[10] formulates the wave control problem in an H_∞ setting, which guarantees a positive real (and, therefore, stabilizing) compensator. Although the causal control compensators are derived using a Wiener-Hopf technique in this work, MacMartin and Hall[10] showed that they may also be derived using state-space techniques.

The structural wave control problem is similar to the active attenuation of acoustics.[15-19] In acoustics, the location of the initial disturbance (primary) is assumed known. Acoustic power can be evaluated by either integrating the far-field power over a closed volume or by evaluating the work performed by the motion of the secondary on the net pressure field. The optimal secondary control action is then determined by minimizing this expression for power, which may also include a control effort term, thereby relating the secondary's response to that of the pressure field or primary response.

The purpose of this paper is to experimentally demonstrate the performance that is theoretically possible using feedback compensators derived using the techniques described by Miller et al.[9] Experimental demonstration verifies the applicability of the techniques while identifying important real world limitations to performance. Compensators for collocated wave control of a Bernoulli-Euler beam, using a moment actuator at the pinned end, are derived. The unconstrained optimal compensator is noncausal and, therefore, not implementable. However, the performance that the noncausal compensator would provide if it were implementable provides a maximum performance limit against which the performances of the implemented compensators are compared. Compensator performance is also compared to that obtained using rate feedback.

This paper starts with a summary of local wave dynamics and power flow, as discussed by Miller and von Flotow.[1] This is followed by a review of junction control, discussed by Miller et al.[9] Compensators for the control of a pinned end of a Bernoulli-Euler beam, using a moment actuator, are derived. This is followed by a description of the experiment setup. Experimental results using four different compensators are compared based on narrow and broadband performance relative to rate feedback and the noncausal compensator. This is concluded by a brief discussion of the difficulties experienced in the implementation of these compensators.

Traveling Wave Dynamics

This section reviews the wave dynamic equations for a structural junction of arbitrary complexity (Fig. 1). The members are modeled as waveguides along which a finite set of decoupled wave modes propagate at each frequency. The member boundaries are modeled as junctions where the waves are coupled through frequency dependent reflection and transmission (scattering) coefficients. The frequency domain derivation of component (member and junction) dynamics was presented by von Flotow.[2] Von Flotow[6] uses an assemblage of member transformation matrices to derive a junction transformation matrix that relates complex wave mode amplitudes on all attached members to the members' cross-sectional quantities. This relation has the form

$$y(\omega) = \begin{Bmatrix} u \\ f \end{Bmatrix} = \begin{bmatrix} Y_{ui} & Y_{uo} \\ Y_{fi} & Y_{fo} \end{bmatrix} \begin{Bmatrix} w_i \\ w_o \end{Bmatrix} = Y(\omega) w(\omega) \tag{1}$$

where $w(\omega)$ is the vector of wave mode amplitudes. This vector is partitioned into incoming (w_i) and outgoing (w_o) waves. The vector y contains all member motions u and stresses f at the interface to the junction.

Junction boundary conditions can be transformed into wave mode coordinates and arranged in a causal, input/output form. Outgoing waves result from the homogeneous scattering of incoming waves and the nonhomogeneous generation by external excitations

$$w_o(\omega) = S(\omega) w_i(\omega) + \psi(\omega) Q(\omega) \tag{2}$$

This description contains only local junction dynamics and does not contain information about other portions of the structure.

Junction Power Flow

Traveling waves result in a flow of power through a structure. Power at an arbitrary member cross section is equal to the product of the deflection velocities and collocated stresses of like type (e.g., rotational rate and moment). The steady-state power flow at a member cross section can be expressed in terms of the spectral components of the response variables using the power theorem, a variation of Parseval's theorem.[20]

Miller and von Flotow[1] expressed the power flow through a junction as

$$P_{\text{avg}}(\omega) = [w_i(\omega)^H \; w_o(\omega)^H] \; P_j(\omega) \begin{bmatrix} w_i(\omega) \\ w_o(\omega) \end{bmatrix} \tag{3}$$

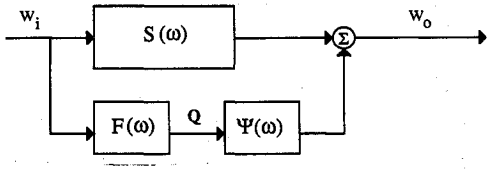

Fig. 2 Feed forward of incoming wave mode amplitudes.

where the submatrices of the junction power flow matrix P_j are given by

$$P_j = \begin{bmatrix} P_{ii} & P_{io} \\ P_{oi} & P_{oo} \end{bmatrix} \tag{4}$$

P_{ii}, P_{oo}, and P_{io} give the power flow associated with incoming waves, outgoing waves, and the interaction between incoming and outgoing waves, respectively. P_{oi} is the Hermitian of P_{io}. P_{avg} is real for any mix of wave modes since P_j is Hermitian.

Junction Control

The incoming waves can be thought of as a disturbance to a junction. Conceptually, the disturbance is measured and fed to the actuators in order to reduce the power associated with the resulting outgoing waves (Fig. 2). This architecture assumes that measurements of the incoming wave mode amplitudes are available.

It is desirable to use cross-sectional variables (e.g., displacement, rotation, bending stress, etc.) as feedback measurements. In the following control formulation, the junction deflections and internal stresses will be redistributed in the cross-sectional state vector such that $\boldsymbol{u}$ contains measurable cross-sectional quantities, whereas $\boldsymbol{f}$ contains those cross-sectional quantities that are commanded by the actuators. Since some combination of cross-sectional states will be commanded by the actuators, the other combination will be available for measurement. Equation (1) can be used to express the amplitudes in $\boldsymbol{u}$ in terms of both incoming and outgoing waves. This results in the feed forward of incoming and the feedback of outgoing wave mode amplitudes (Fig. 3). Rearrangement of the block diagram in Fig. 3 yields a structure identical to that in Fig. 2 (see Fig. 4). This illustrates that cross-sectional variables can be used as feedback measurements to mimic the feed forward of incoming wave mode amplitudes.

For control purposes, a combination of power flow and control effort will be minimized. Outgoing power is defined as positively flowing so that power minimization corresponds to maximizing power absorption. Since power flow is expressed in terms of its frequency components, a frequency domain formulation is used. Adding a quadratic control effort penalty R to the power term in Eq. (3) and taking the expected value of the resulting integral relation gives the cost functional as

$$\begin{aligned} J &= \frac{1}{2} E\left\{\int_{-\infty}^{\infty} \left(\boldsymbol{w}^H P_j \boldsymbol{w} + \boldsymbol{Q}^H R \boldsymbol{Q}\right) \mathrm{d}\omega\right\} \\ &= \frac{1}{2}\int_{-\infty}^{\infty} \text{trace}\left[E\left(P_j \boldsymbol{w}\boldsymbol{w}^H + R\boldsymbol{Q}\boldsymbol{Q}^H\right)\right] \mathrm{d}\omega \\ &= \frac{1}{2}\int_{-\infty}^{\infty} \text{trace}\left[P_j(\omega)\Phi_{ww}(\omega) + R(\omega)\Phi_{QQ}(\omega)\right] \mathrm{d}\omega \end{aligned} \tag{5}$$

where the assumed power spectral densities of the wave modes and control effort are

$$\Phi_{ww}(\omega) = E(\boldsymbol{w}\boldsymbol{w}^H), \qquad \Phi_{QQ}(\omega) = E(\boldsymbol{Q}\boldsymbol{Q}^H) \tag{6}$$

The power spectral density Φ_{QQ} can be expressed in terms of $\Phi_{w_i w_i}$ (Fig. 4) as

$$\Phi_{QQ} = E(\boldsymbol{Q}\boldsymbol{Q}^H) = E(HK\boldsymbol{w}_i\boldsymbol{w}_i^H K^H H^H) = HK\Phi_{w_i w_i} K^H H^H \tag{7a}$$

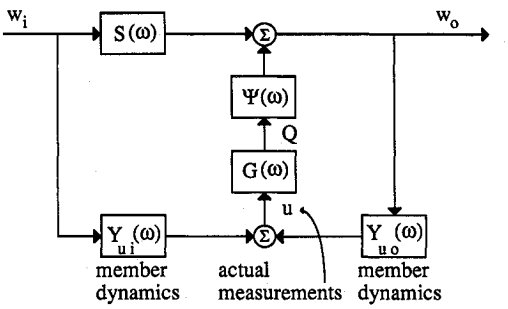

Fig. 3 Feedback of cross-sectional measurements.

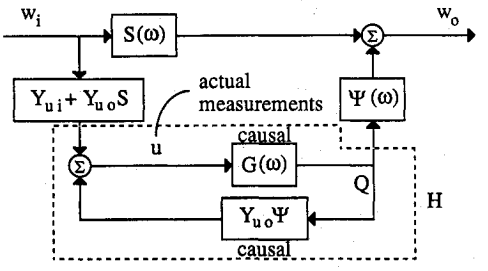

Fig. 4 Feedback of cross-sectional measurements to mimic the feed forward of incoming wave mode amplitudes.

where K is defined as

$$K = Y_{ui} + Y_{uo}S \tag{7b}$$

from Fig. 4. H is the transfer function of the elements contained within the dashed area in Fig. 4 and will be referred to as the feed-forward compensator.

To minimize the cost, consider small perturbations of the feed-forward compensator

$$H(\omega) \Rightarrow H(\omega) + \epsilon\eta(\omega) \tag{8}$$

where ϵ is a small parameter and $\eta(\omega)$ is the frequency dependent perturbation. The first variation of the cost is then given by

$$\begin{aligned} \partial J = \int_{-\infty}^{\infty} \text{Re}\,(\text{trace}\{&\eta^H[\psi^H(P_{oi} + P_{oo}S) \\ &+ (\psi^H P_{oo}\psi + R)HK]\Phi K^H\})\,\mathrm{d}\omega \end{aligned} \tag{9}$$

where the real part of the trace is retained. For brevity, Φ is used in place of $\Phi_{w_i w_i}$ in Eq. (9) and for the following analysis. The first variation must be zero at an optimum for all admissible perturbations. At this point, the optimization procedure can proceed in several directions depending on the perturbations allowed.

Noncausal Solution

Since the optimal noncausal solution is sought, no constraint is placed on perturbations to H. Therefore, the optimal gain matrix H must make Eq. (9) satisfy

$$\partial J = 0 \tag{10}$$

for any arbitrary perturbation given by η^H. This indicates that η, and, therefore, the feed-forward compensator H, may contain both right and left half complex plane dynamics.

Equation (10) is satisfied if

$$HK = -(\psi^H P_{oo}\psi + R)^{-1}\psi^H[P_{oi} + P_{oo}S] = F \tag{11}$$

Equation (11) gives the compensator (F in Fig. 2) that feeds the incoming wave mode amplitudes to the control actuators. The gain matrix G in Fig. 4 that feeds cross-sectional junction motions to control inputs, and represents the implemented compensator can be found by solving Eq. (11) for H and substituting into

$$G = (I + HY_{uo}\psi)^{-1}H \tag{12}$$

This procedure minimizes power flow frequency by frequency and provides no guarantee that the compensator will be causal or implementable. Therefore, the next two sections discuss techniques for finding causal solutions.

Causal, Fixed-Form Parameter Optimization

The first step is to select a causal compensator form with a variable gain

$$H(s) = \alpha\, h(s) \tag{13}$$

This form is then substituted into Eqs. (5) and the trace is minimized with respect to the variable gain α. The compensator $G(s)$ is again found using Eq. (12). The effectiveness of the compensator depends on the insight of the designer in the selection of $h(s)$.

Causal Solution Using Wiener-Hopf Techniques

The following discussion on the Wiener-Hopf (W-H)[21] technique is summarized from Miller et al.[9] The fundamental difference between the W-H and noncausal solutions is the definition of allowable perturbations. In the noncausal solution, the perturbing matrix η was permitted to be arbitrary. In the problem at hand, G must be causal. From Eq. (12), the feed-forward compensator matrix H can be expressed as

$$H = G(I + Y_{uo}\psi G)^{-1} \tag{14}$$

Since G and $Y_{uo}\psi$ are causal, H must be also. Furthermore, H must be stable since an unstable feed-forward compensator will result in unbounded outgoing wave mode amplitudes and, therefore, infinite cost. Hence, $H(s)$ must be analytic in the right half of the complex plane [i.e., right half plane analytic (RHPA)]. Thus, the matrix $\eta(s)$, which perturbs $H(s)$ from its optimal form, must itself be causal and, therefore, RHPA. Note, in Eq. (9), that the perturbation shows up as $\eta^H(j\omega)$. The analytic continuation of $\eta^H(j\omega)$ in the complex plane is given by $\eta(-s)$. For simplicity, we define

$$\eta^H(s) = \eta(-s) \tag{15}$$

Thus, η^H must be left half plane analytic (LHPA).

The optimal H_{RHPA}, for arbitrary LHPA perturbations in η^H, must cause

$$[\psi^H(P_{oi} + P_{oo}S) + (\psi^H P_{oo}\psi + R)H_{\text{RHPA}}K]\Phi K^H \tag{16}$$

to be LHPA. If left half plane singularities do exist in this expression, then the integral in Eq. (9), when the contour is closed about the left half plane, will be nonzero for some RHPA η and the stationary cost constraint [Eq. (10)] will not be satisfied. Therefore, the expression in Eq. (16) must be equal to some LHPA function, so that

$$\psi^H(P_{oi} + P_{oo}S)\Phi K^H + (\psi^H P_{oo}\psi + R)H_{\text{RHPA}}K\Phi K^H = A_{\text{LHPA}} \tag{17}$$

The W-H technique proceeds as follows. It is observed that Eq. (17) has the form

$$H_N + H_D H_{\text{RHPA}} H_C = A_{\text{LHPA}} \tag{18}$$

Solving the RHPA part of this relation for H_{RHPA} gives

$$H_{\text{RHPA}} = -H_{D\,\text{RHPA}}^{-1}[\text{PTF}(H_{D\,\text{LHPA}}^{-1}H_N H_{C\,\text{LHPA}}^{-1})]H_{C\,\text{RHPA}}^{-1} \tag{19}$$

where PTF(.) denotes the positive time function of its argument. That is, the argument is split into the sum of two parts: a LHPA and a RHPA part. The positive time function is the RHPA portion. The final step involves evaluating G using H_{RHPA} from Eq. (19) in place of H in Eq. (12). Given that future information is not available to the controller, a reduction in performance over the noncausal case is expected.

Experiment Control Formulation

This section derives the various junction controllers used in the experiments. Noncausal, causal fixed-form, W-H, W-H positive real approximation, and rate feedback compensators are applied to the left, pinned end of a dispersive, undamped, uniform, Bernoulli-Euler beam (Fig. 5). The governing partial differential equation is

$$EI\frac{\partial^4 v}{\partial x^4} + \rho A\frac{\partial^2 v}{\partial t^2} = 0 \tag{20}$$

where E, I, ρ, and A are the modulus of elasticity, area moment of inertia, volume density of mass, and cross-sectional area, respectively, and $v(x,t)$ is the transverse displacement coordinate. In Fig. 5, $x = 0$ at the pinned end. From the dispersion relation, the wave number k is expressed in terms of the complex Laplace variable s as

$$k = \sqrt[4]{\rho A/EI}\,\sqrt{\omega} = c_0\sqrt[4]{s}\,\sqrt[4]{-s} \tag{21}$$

Notice that the right side of Eq. (21), $k(s)$, is the analytic continuation, throughout the complex plane, of the function on the left side, $k(\omega)$, which is valid on the imaginary axis.

The motion of the waveguide, as composed of wave modes supported by the partial differential equation in Eq. (20), is given by

$$v(x,t) = w_{tp}\exp[\pm ikx + i\omega t] + w_{rp}\exp[\pm(-ikx) + i\omega t]$$
$$+ w_{re}\exp[-kx + i\omega t] + w_{te}\exp[kx + i\omega t] \tag{22}$$

The $+/-$ symbol preserves the propagation direction when ω is positive or negative. For brevity, this notation will be truncated to include only the upper sign. Using Eq. (22), the junction transformation [Eq. (1)] is

$$\begin{Bmatrix} v' \\ -EIv''' \\ v \\ EIv'' \end{Bmatrix} = \begin{bmatrix} ik & k & -ik & -k \\ iEIk^3 & -EIk^3 & -iEIk^3 & EIk^3 \\ 1 & 1 & 1 & 1 \\ -EIk^2 & EIk^2 & -EIk^2 & EIk^2 \end{bmatrix} \begin{Bmatrix} w_{tp} \\ w_{te} \\ w_{rp} \\ w_{re} \end{Bmatrix} \tag{23}$$

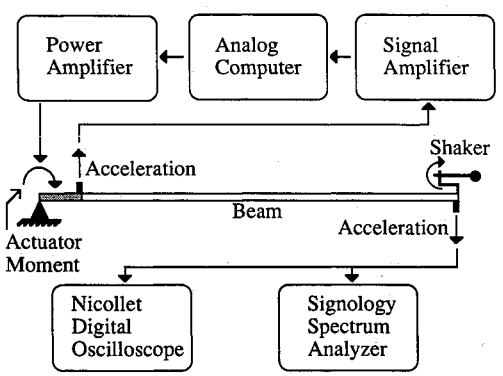

Fig. 5 Experiment setup.

where w_{lp} is the leftward propagating, incoming wave; w_{le} the leftward emanating evanescent, incoming wave; w_{rp} the rightward propagating, outgoing wave; and w_{re} the rightward emanating evanescent, outgoing wave.

The scattering matrix for a pinned boundary condition is

$$S = \begin{bmatrix} -1 & 0 \\ 0 & -1 \end{bmatrix} \tag{24}$$

The wave generation matrix and assumed incoming wave mode spectrum are

$$\psi = \frac{1+i}{2EIk^3}\begin{bmatrix} 1 & -k \\ 1 & -ik \end{bmatrix}, \qquad \psi_M = \frac{1}{2EIk^2}\begin{Bmatrix} -1 \\ 1 \end{Bmatrix} \tag{25}$$

$$\Phi = \frac{a^2}{(s-\omega_n)^2}\begin{bmatrix} 1 & 0 \\ 0 & 1 \end{bmatrix}\frac{a^2}{(s+\omega_n)^2} \tag{26}$$

where ψ_M is the wave generation matrix with only moment actuation (no force). The junction power matrix is

$$P_j = 4\omega k^3 EI \begin{bmatrix} -1 & 0 & 0 & 0 \\ 0 & 0 & 0 & i \\ 0 & 0 & 1 & 0 \\ 0 & -i & 0 & 0 \end{bmatrix} \tag{27}$$

Noncausal Solution

If only moment actuation is used, cheap control can be derived ($R = 0$). The noncausal feedback matrix in terms of cross-sectional measurements [Eqs. (11) and (12)] is

$$M = \sqrt{2}c_0 EI\sqrt{-s}\,[1\ \ 0]\begin{Bmatrix} v' \\ -EIv''' \end{Bmatrix} \tag{28a}$$

where

$$c_0 = \sqrt[4]{\rho A/EI} \tag{28b}$$

This calls for endpoint rotation feedback and does so through a frequency dependent compensator, which is similar to a half differentiator, but shifted 90 deg. The compensator is optimized frequency by frequency and is, therefore, independent of the incoming wave mode spectrum.

The primary drawback to this solution is that the compensator is noncausal. Although a half differentiator can be approximated,[6] a 90-deg phase shifter cannot. Therefore, a causal solution is required.

Fixed-Form Solution

This solution illustrates the use of a causal fixed-form parameter optimization technique. The form of the noncausal compensator in Eqs. (28), shifted 90 deg, will be used. Minimizing the cost with respect to a variable gain yields

$$M = \sqrt{2}c_0 EI\sqrt{s}\,[1\ \ 0]\begin{Bmatrix} v' \\ -EIv''' \end{Bmatrix} \tag{29}$$

Notice that the gain equals that in Eqs. (28).

Wiener-Hopf Solution

The feedback, found using Eqs. (19) and (12), is

$$M = -c_0 EI\left(\sqrt{2}\sqrt{s} - \frac{8s^{7/4}}{(\omega_n + 5s)\sqrt[4]{\omega_n}}\right)[1\ \ 0]\begin{Bmatrix} v' \\ -EIv''' \end{Bmatrix} \tag{30}$$

Notice that if the compensator in Eq. (30) were altered to represent the feedback of rotational velocity to external moment (G/s), the new compensator would not be positive real at all frequencies. At low frequencies, where the left part of the term in parentheses dominates, the compensator would be negative real and lead to the generation of power at the active junction. This could lead to instability.

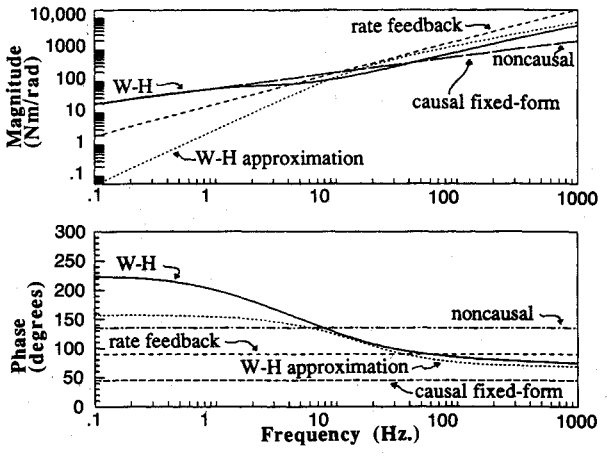

Fig. 6 Magnitude and phase of the various feedback compensator transfer functions.

Figure 6 compares the transfer functions of the noncausal, causal fixed-form, and W-H solutions. For the W-H solution, the corner frequency Φ was chosen as $\omega_n = 6.4$ Hz because this frequency corresponds to a resonant frequency of the structure. Notice that this selection implies knowledge of the resonant behavior that is not captured in the control design model. Near this frequency, the W-H solution has half the magnitude and the same phase as the noncausal solution. The W-H solution is better than the causal fixed-form solution at mimicking the noncausal solution near the frequencies of importance.

Positive Real Approximation to Wiener-Hopf Solution

A positive real approximation to Eq. (30) is required to guarantee stability without knowledge of the structure's resonant behavior. This W-H approximation should mimic the W-H solution in the frequency range in which Eq. (30) is positive real (above 2 Hz). Looking at the right term in Eq. (30), the high frequency $s^{3/4}$ behavior and gain ($8c_0EI/5\omega_n{}^{1/4}$) are used in the approximation

$$M = \frac{8c_0 EI}{5\sqrt[4]{\omega_n}}\frac{s^2}{s+92}\frac{1}{\sqrt[4]{s}}[1\ \ 0]\begin{Bmatrix} v' \\ -EIv''' \end{Bmatrix} \tag{31}$$

The first-order pole in Eq. (31) maintains the phase between 67.5 and 157.5 deg (positive real). The corner frequency of 92 rad/s provides the best match with the W-H phase. The transfer function of Eq. (31) is shown in Fig. 6. This W-H approximation is used in place of the W-H compensator for the duration of this paper.

Rate Feedback

For comparison purposes, rate feedback is analyzed and band-limited rate feedback is experimentally implemented. The gain that maximizes damping in a mode at 10 Hz is used. The gain, determined by analyzing transfer functions of the mathematical model, is

$$M = 3s\,[1\ \ 0]\begin{Bmatrix} v' \\ -EIv''' \end{Bmatrix} \tag{32}$$

The magnitude and phase are shown in Fig. 6.

Theoretical Open- and Closed-Loop Transfer Functions

Using the phase closure principle described by Miller and von Flotow,[1] a transfer function can be derived between force and transverse displacement at the opposite, free end of the

Table 1 Beam properties

Length	7.32 m
Width	10.20 cm
Thickness	0.3175 cm
EI	31.1 N m^2
ρA	2.85 kg/m
Damping ratio averages 0.30% below 30 Hz	

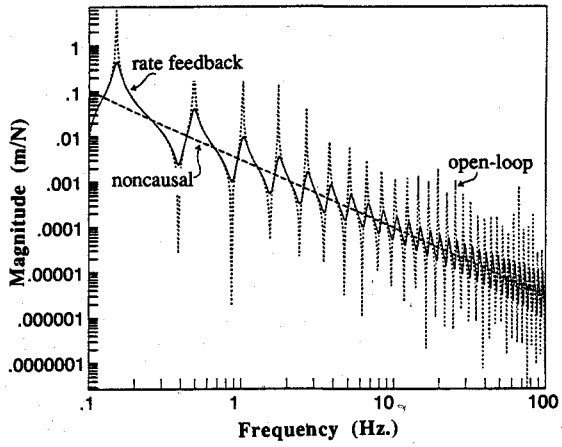

Fig. 7 Beam transfer function in open loop, using rate feedback and the noncausal compensator.

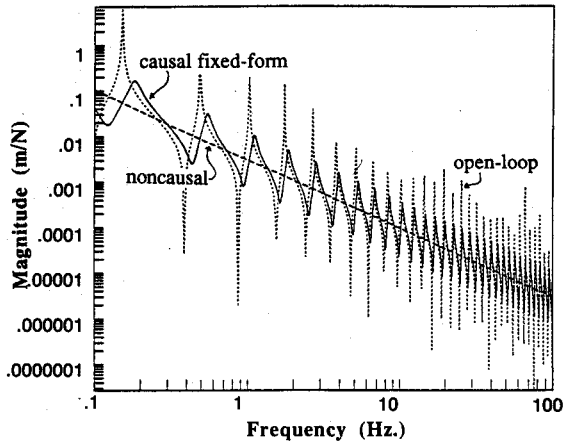

Fig. 8 Beam transfer function in open loop, using the causal, fixed-form compensator and the noncausal compensator.

beam. The beam properties are given in Table 1. Figure 7 compares the open-loop magnitude characteristics with those obtained using rate feedback and the noncausal compensator. For rate feedback, notice that damping is a function of frequency. Below 10 Hz, the gain is lower than optimal. Above 10 Hz, the gain is higher than optimal. The latter leads to clamping of the pinned end at high frequencies. This transfer function is provided as a comparison for the performance of the wave control compensators. The noncausal compensator reflects no incoming propagating waves as outgoing propagating waves. This feature essentially eliminates resonant behavior and the beam behaves as if it were semi-infinite. This represents the best performance that is theoretically possible.

Figure 8 shows the magnitude characteristics obtained using the causal fixed-form compensator. The selected form of the compensator causes the damping to be independent of frequency. Although the damping performance in the neighborhood of 10 Hz is less than that obtainable using rate feedback, the causal fixed-form compensator absorbs the same fraction of power at all frequencies. Since the amount of power absorbed using rate feedback decreases with increasing frequency, the damping provided by the causal fixed-form compensator is more broadband.

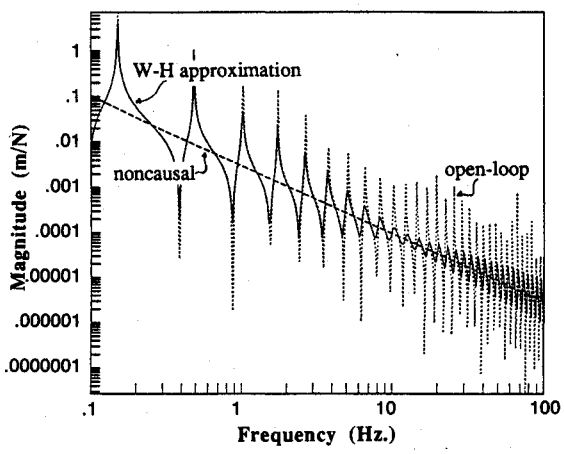

Fig. 9 Beam transfer function in open loop, using the W-H approximation and the noncausal compensator.

Table 2 Control hardware properties

Torque actuator	
Manufacturer/model	PMI U-9
Torque constant	0.0212 N m/A
Armature plus arm inertia	0.000146 Kg m^2
Motor diameter	0.1048 m
Motor thickness	0.0345 m
Current source	EG&G PA-601
Gain	−2.08 A/V
Piezo resistive accelerometer	
Manufacturer/model	Endevco 2262-25
Excitation voltage	10.00 V
Gain with amplifier	2.86 V/m/s^2
Corner frequency	1180 Hz
Damping	light
Distance from motor pivot	0.062 m

Figure 9 shows the transfer function obtained using the W-H approximation. Notice the significant increases in damping near $\omega = 10$ Hz. Of the three compensators, the W-H approximation provides the best narrow-band performance because it provides a better approximation of the noncausal compensator near 10 Hz. On the other hand, the damping performance is lower for the W-H approximation than for the fixed-form compensator outside the frequency range of interest. In general, as more narrow-band performance is achieved, broadband performance is sacrificed. Recent results by MacMartin and Hall[10] suggest that this trade-off in performance can be succinctly described in an H_∞ setting.

Experiment Setup

This section describes the hardware components used in the experiments. These components are the structure, the control hardware, the control computer, and the shaker and sensor used to measure the open- and closed-loop transfer functions. Finally, the experiment protocol is described. Figure 5 shows the experiment's functional elements.

Structural Characteristics

The controlled structure is a 24-ft brass beam, suspended from six pairs of wire, with its longitudinal axis horizontal (Table 1). The suspension wires attach to the beam at one-seventh length intervals with the two beam ends left free for the attachment of the control and shaker hardware.

Control Hardware Characteristics

The control hardware consists of the control actuator and the sensor used to obtain the feedback measurement. A PMI motor with a low inertia, laser etched armature was chosen. The armature was clamped to the beam with the permanent

magnet clamped to the laboratory frame. This replicates the pinned condition used in the model. Although the actuator is not space realizable, the control formulation is equally valid for space-realizable actuators. The specifications for the actuator and sensor are listed in Table 2, and a drawing of the hardware attached to the beam end is shown in Fig. 10.

Control Computer

The control computer is a PACE TR-48 analog computer. The two types of fractional elements used in the experiment are a half integrator ($1/s^{1/2}$) described by von Flotow and Schafer[7] and a quarter integrator ($1/s^{1/4}$) described by Carlson and Halijak.[22] The circuit approximations exhibited good accuracy from 0.1 to 1000 Hz.

Shaker and Sensor Hardware

Shaker and sensor hardware are attached to the other end of the beam for acquisition of transfer function data. The shaker is a pivoting proof-mass actuator[23] that predominantly exerts force, and the sensor is a linear accelerometer measuring transverse beam acceleration. The specifications are given in Table 3. Therefore, during open- and closed-loop tests, the left end of the beam is controlled while the transfer function data is acquired at the right end from shaker input voltage to the output voltage of the collocated, linear accelerometer. This data is divided by the frequency squared and appropriate gain factors to obtain force to displacement transfer functions consistent with the analysis.

Experiment Protocol

The open-loop transfer function is measured for a frequency range of 0.5–50 Hz. Then, for each feedback compensator used, the following iterative procedure is followed. First, a circuit gain, variable between 0 and 1, is increased until the onset of instability or the arrival at the optimal gain. In the event of instability, the cause is identified. This consists of identifying the frequency of the instability and either identifying control hardware with dynamics at that frequency, measuring the loop transfer function in that frequency range to investigate phase and/or gain margin problems, or simply speculating as to the origin of the instability. Once eliminated through filtering or hardware adjustment, the procedure is repeated, often leading to the identification of another instability at hopefully higher gain. If the optimal gain is reached, or an instability cannot be eliminated after a reasonable amount of effort, the transfer function of the beam is measured.

Often the instabilities originate from unforeseen causes. Rather than attempt to model all possible details that could lead to instability, a more efficient approach is to conduct the experiment and identify those characteristics that actually do lead to instability. If the experiment is never conducted, details that are obscure during open-loop testing might never be identified until the loop is closed in an operational environment.

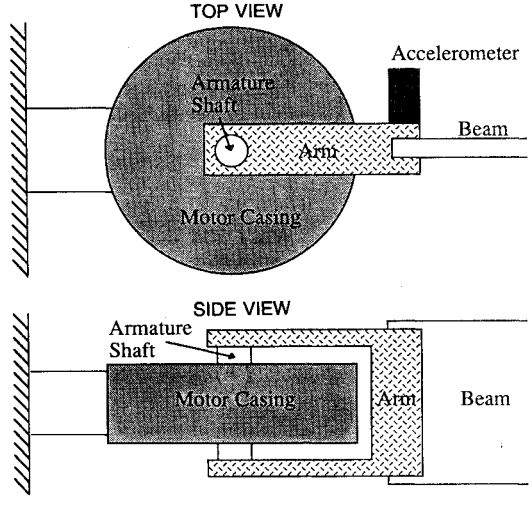

Fig. 10 Top and side views of the control hardware.

Table 3 Shaker and sensor properties

Shaker's DC servo motor	
Manufacturer/model	Pittman 7214
Torque constant	0.0357 N m/A
Current source	EG&G PA-223
Gain with amplifier	−1.87 A/V
Piezo resistive accelerometer	
Manufacturer/model	Endevco 2262-25
Gain	0.378 V/m/s^2

Experimental Results

The feedback compensators and results of five tests are summarized in this section. The first test consists of obtaining the transfer function of the beam in open loop. The second test uses the causal, fixed-form compensator to control the beam. The third test acquires the same information for the beam controlled using rate feedback. The fourth test involves the implementation of the W-H approximation. This compensator exhibits the same characteristics as the W-H compensator in the frequency range of interest but is positive real and, therefore, has certain stability guarantees. The fifth test involves implementing the highest stable gain using the W-H approximation. In the following discussion, the results of these five tests are compared using measured transfer functions.

Feedback Compensators

Three different compensators are implemented. Since the feedback measurement is of rotational acceleration, the implemented compensators are good approximations of the analytical compensators, between 0.5 and 50 Hz, scaled by the frequency squared.

The rate feedback compensator is given by

$$\frac{M(s)}{s^2\nu'(s)} = 0.31^* \frac{10s}{s^2 + 0.889s + 0.394} * \frac{628}{s + 628} \tag{33}$$

The middle portion is a stabilized integrator with a corner frequency of 0.1 Hz and a damping ratio of 0.7071. This filters and integrates frequencies below and above 0.1 Hz, respectively. The right portion contains a first-order filter to eliminate an instability, at 1180 Hz, caused by the lightly damped feedback accelerometer.

The causal, fixed-form compensator is given by

$$\frac{M(s)}{s^2\nu'(s)} = 0.94^* \frac{10s}{s^2 + 0.889s + 0.394} * \frac{2.58}{\sqrt{s}} \tag{34}$$

Again, the middle term is a stabilized integrator and the right term is a half integrator implemented using a rational approximation from 0.1 to 1000 Hz. This approximation is realized by a repeated lattice structure in the feedback path of an operational amplifier.[7]

The W-H approximation is given by

$$\frac{M(s)}{s^2\nu'(s)} = 0.039^* \frac{92}{s + 92} * \frac{700}{s + 700} * \frac{3.348}{\sqrt[4]{s}} \tag{35}$$

The left term is the first-order pole shown in Eq. (31). The middle term is a low pass filter and the right term is a quarter integrator realized using a nonrepeated resistor and capacitor network in the feedback path of an operational amplifier.[22]

The actual compensators were built to be good approximations of the ideal compensators in the frequency range of

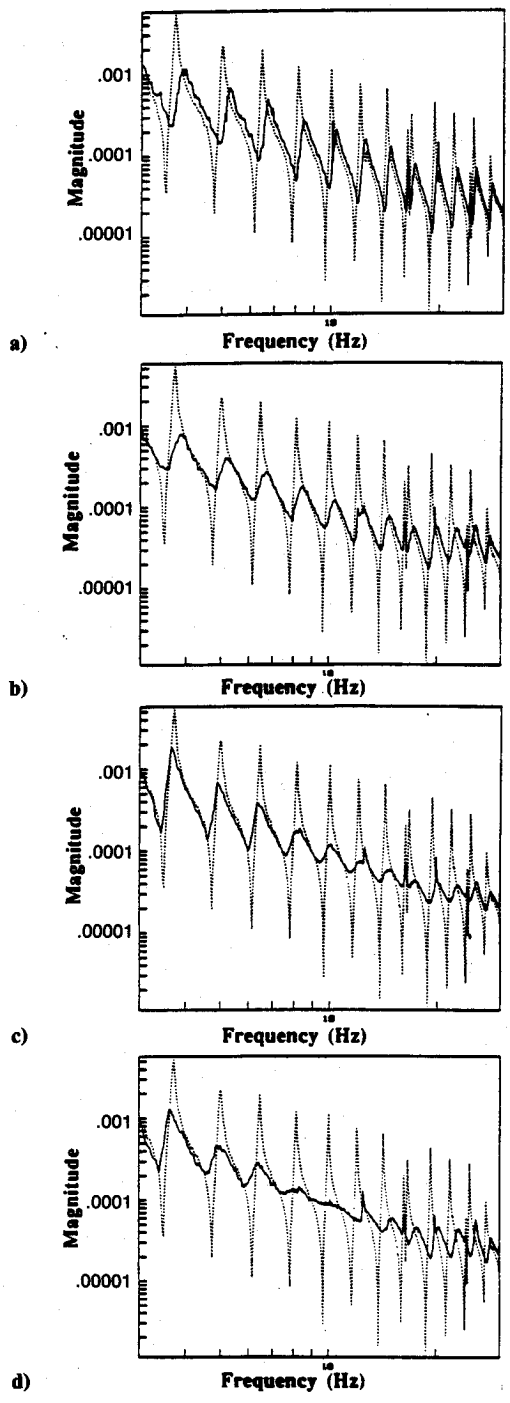

Fig. 11 Measured open- and closed-loop transfer functions using a) the causal, fixed-form compensator; b) rate feedback; c) the W-H approximation at optimal gain; and d) the W-H approximation at 1.55 times optimal gain.

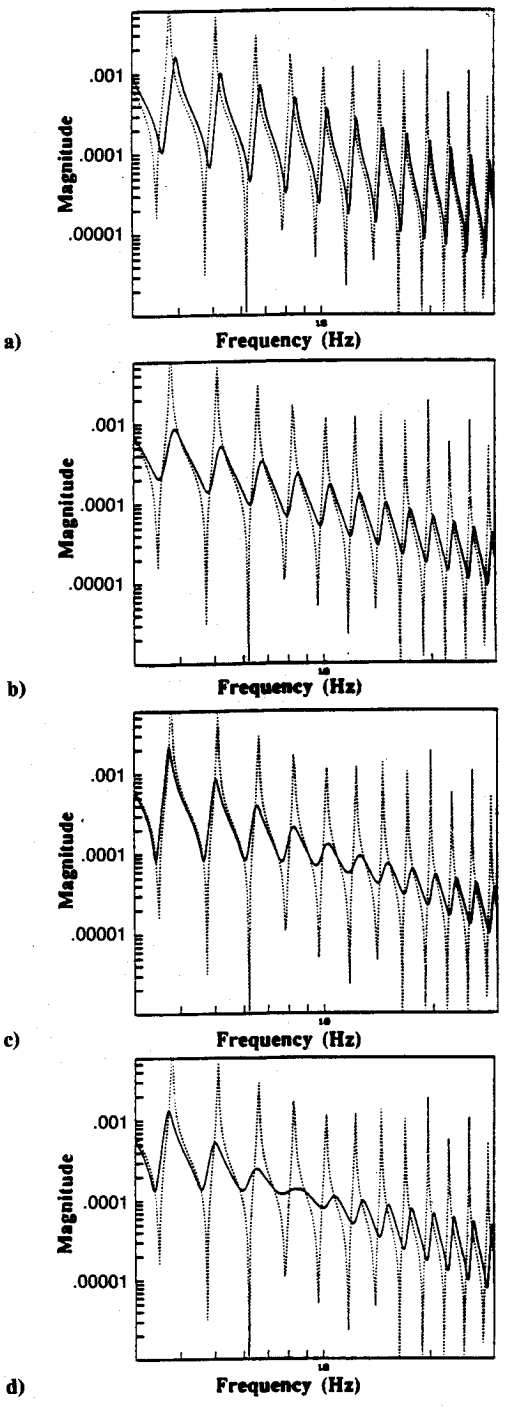

Fig. 12 Model's open- and closed-loop transfer functions using a) the causal, fixed-form compensator; b) rate feedback; c) the W-H approximation at optimal gain; and d) the W-H approximation at 1.55 times optimal gain.

interest (0.1–1000 Hz). These compensators were implemented. Since all instabilities that occurred at levels of gain lower than optimal were suppressed without altering the compensator characteristics, no consideration was given to closed-loop behavior in the compensator roll-off frequency range. This is fortunate since little roll-off could be added without exhausting phase margin.

Instabilities that did occur at low gain, caused by motor mount dynamics and observation spillover from a torsion mode, were suppressed by making minor hardware adjustments. The tests were then repeated at the optimal levels of damping with no further consideration of roll-off dynamics. Identification and suppression of the instabilities is discussed in more detail in the Performance Limitations section.

This debugging procedure illustrates the importance of conducting experiments to identify those dynamic characteristics that are important to the control design. This process often involves such a trade-off between modeling effort and technical return. More consideration of roll-off characteristics would be required to insure stability robustness.

Random Excitation Tests

Figures 11 show the measured transfer functions for the five different tests. Figures 12 show the predicted transfer functions. Open- and closed-loop curves are dotted and solid, respectively. Notice that the model, based on measured values

of EI, ρA, and length, predicts open-loop poles and zeroes within 4% of their measured frequencies.

Figure 11a compares the open- and closed-loop transfer functions of the beam using the causal, fixed-form compensator at the optimal gain. Although this solution exhibits a more broadband effect than the rate feedback, it is achieved by sacrificing narrow-band damping performance. Notice that torsional modes appear in the data above 10 Hz. Figure 12a compares the equivalent model transfer functions. Although the experimental data indicates damping performance that is independent of frequency, the level of damping appears to exceed that predicted. This may result from greater open-loop damping in the actual beam than in the model, due to either material damping in the beam or friction in the shaker. The level of damping in the model is not based on the damping mechanisms in the actual structure except to the extent that it is light.

Figure 11b shows the closed-loop transfer function using rate feedback. As supported by the model's transfer function (Fig. 12b), rate feedback provides better narrow-band damping performance than the causal, fixed-form compensator. It is difficult, however, to judge the broadband behavior using this narrow frequency range.

Figure 11c shows the closed-loop transfer function using the W-H approximation given in Eq. (35) at the optimal gain. In the frequency range of 10–20 Hz, the damping performance exceeds that shown in Figs. 11a and 11b. Notice that the high frequency decrease in damping is perceptible. Figure 12c displays the model's transfer function.

Figure 11d shows the closed-loop transfer function using the W-H approximation with a gain that is 1.55 times larger than the optimal gain. As shown in Fig. 6, this causes the W-H compensator to better replicate the noncausal compensator. The mode near 6.4 Hz has been practically eliminated. Between 8 and 10 Hz, the closed-loop magnitude approaches a line with a slope of $-3/2$. The model transfer function (Fig. 12d) at this gain predicts a slightly different behavior. This could result from the small amount of additional lag in the implemented compensator when compared with Eq. (35).

Of the compensators implemented, the W-H approximation provided the most damping in a single mode. The causal, fixed-form performance is broadband, whereas rate feedback makes the transition from damping to clamping with increasing gain, without ever achieving a gain and phase equal to that of the noncausal compensator.

Performance Limitations

The lowest gain instability was caused by the lightly damped feedback accelerometer with a resonance at 1180 Hz. This was suppressed with a first-order, low pass filter. The second encountered instability was due to the flexibility of the angle iron frame to which the actuator's permanent magnet was attached. This flexibility caused the permanent magnet of the torque actuator to undergo rotation. This allowed the feedback sensor to measure acceleration in the absence of armature rotation with respect to the permanent magnet. In other words, the accelerometer and motor were no longer a dual sensor/actuator pair. This instability was suppressed by placing a layer of viscoelastic foam between the frame and laboratory floor. This contributed insignificant damping to the beam modes between 0.5 and 50 Hz. The third encountered instability was caused by the feedback accelerometer measuring torsional acceleration. This was suppressed by placing the accelerometer closer to the centerline of the beam.

Once these three instabilities were suppressed, the rate feedback, causal fixed-form, and W-H compensators were implemented at their optimal gains. The W-H approximation with 1.55 times higher gain (Fig. 11d) was at the highest stable gain achieved using the W-H approximation. An instability at 773 Hz near the frequency of the 80th bending mode, believed to be caused by torsional modes, was not suppressed.

Conclusions

If the control objective is to extract energy from the structure, maximizing power absorption frequency by frequency provides the best solution. As shown, however, there is no guarantee that this compensator will be implementable, raising the need for causal solutions. Two alternative techniques were illustrated for finding causal compensators under given hardware constraints. The Wiener-Hopf approach was shown to provide better narrow-band damping performance than rate feedback without perceptible degradation in broadband damping performance. This was achieved because the Wiener-Hopf technique more closely mimics the magnitude and phase of the noncausal compensator. The limitation to the Wiener-Hopf procedure is that it does not guarantee that the compensator has a positive real form. Therefore, a positive real approximation to the Wiener-Hopf compensator was derived, using engineering insight. Further work is needed to constrain the Wiener-Hopf formulation to yield a positive real compensator. This Wiener-Hopf approximation was implemented experimentally and achieved predicted levels of damping. These levels of damping were shown to far exceed the levels of damping that could be achieved through rate feedback. Limitations to performance included the discovery of frequencies above which the sensor and actuator were no longer dual and the inadvertent coupling of the control hardware to unmodeled torsion modes in the structure.

Acknowledgments

This research was supported by NASA under the grant supporting the Space Engineering Research Center at the Massachusetts Institute of Technology. Special thanks to Mr. Paul Bauer for his invaluable assistance in making the experiment work.

References

[1]Miller, D. W., and von Flotow, A. H., "A Travelling Wave Approach to Power Flow in Structural Networks," *Journal of Sound and Vibration,* Vol. 128, No. 1, 1989, pp. 145–162.

[2]Von Flotow, A. H., "Disturbance Propagation in Structural Networks," *Journal of Sound and Vibration,* Vol. 106, No. 3, 1986, pp. 433–450.

[3]Signorelli, J., and von Flotow, A. H., "Wave Propagation, Power Flow, and Resonance in a Truss Beam," *Journal of Sound and Vibration,* Vol. 126, No. 1, Nov. 1988, pp. 127–144.

[4]Hagedorn, P., and Schmidt, J. T., "Active Vibration Damping of Flexible Structures Using the Traveling Wave Approach," *Proceedings of the Second International Symposium on Spacecraft Flight Dynamics,* Oct. 1986, European Space Agency, SP-255, Dec. 1986, pp. 47–52.

[5]Von Flotow, A. H., and Schafer, B., "Wave-Absorbing Controllers for a Flexible Beam," *Journal of Guidance, Control, and Dynamics,* Vol. 9, No. 6, 1986, pp. 673–680.

[6]Von Flotow, A. H., "Traveling Wave Control for Large Spacecraft Structures," *Journal of Guidance, Control, and Dynamics,* Vol. 9, No. 4, 1986, pp. 462–468.

[7]Von Flotow, A. H., and Schafer, B., "Experimental Comparison of Wave Absorbing and Modal Based Low-Authority Controllers for a Flexible Beam," *Proceedings of the AIAA Guidance and Control Conference,* AIAA, New York, Aug. 1985, pp. 1–10.

[8]Miller, D. W., von Flotow, A. H., and Hall, S. R., "Active Modification of Wave Reflection and Transmission in Flexible Structures," *Proceedings of the American Control Conference,* Vol. 2, American Automatic Control Council, Green Valley, AZ, June 1987, pp. 1318–1324.

[9]Miller, D. W., Hall, S. R., and von Flotow, A. H., "Optimal Control of Power Flow at Structural Junctions," *Journal of Sound and Vibration,* Vol. 140, No. 3, 1990, pp. 475–497.

[10]MacMartin, D., and Hall, S. R., "An H_∞ Power Flow Approach to Control of Uncertain Structures," *Journal of Guidance, Control, and Dynamics* (to be published).

[11]Mace, B. R., "Active Control of Flexural Vibrations," *Journal of Sound and Vibration,* Vol. 114, No. 2, 1987, pp. 253–270.

[12]Redman-White, W., "Experiments on the Active Control of Flexural Wave Power Flow," *Journal of Sound and Vibration,* Vol. 112, No. 1, 1987, pp. 187–191.

[13]Pines, D. J., "Active Control of Bending Waves at Acoustic Frequencies," S.M. Thesis, Massachusetts Inst. of Technology, Cambridge, MA, 1988.

[14]Scheuren, J., "Active Control of Bending Waves in Beams," *Proceedings of Internoise,* Wirtschaftsverlag NW, D-Brewerhaven, Germany, Sept. 1985, pp. 591–594.

[15]Nelson, P. A., Curtis, A. R. D., Elliott, S. J., and Bullmore, A. J., "The Minimum Power Output of Free Field Point Sources and the Active Control of Sound," *Journal of Sound and Vibration,* Vol. 116, No. 3, 1987, pp. 397–414.

[16]Nelson, P. A., Curtis, A. R. D., Elliott, S. J., and Bullmore, A. J., "The Active Minimization of Harmonic Enclosed Sound Fields, Part I: Theory," *Journal of Sound and Vibration,* Vol. 117, No. 1, 1987, pp. 1–13.

[17]Elliot, S. J., and Nelson, P. A., "Multichannel Active Sound Control Using Adaptive Filtering," *1988 Proceedings of the ICASSP,* pp. 2590–2593.

[18]Elliot, S. J., Stothers, I. M., Nelson, P. A., "A Multiple Error LMS Algorithm and its Application to the Active Control of Sound and Vibration," *IEEE Transactions on Acoustics, Speech and Signal Processing,* ASSP-35, Oct. 1987, pp. 1423–1435.

[19]Eriksson, L. J., Allie, M. C., Greiner, R. A., "The Selection and Application of an IIR Adaptive Filter for use in Active Sound Attenuation," *IEEE Transactions on Acoustics, Speech and Signal Processing,* ASSP-35, April 1987, pp. 433–437.

[20]Bracewell, R. N., *The Fourier Transform and Its Applications,* 2nd ed., McGraw-Hill, New York, 1978.

[21]Brown, R. G., *Introduction to Random Signal Analysis and Kalman Filtering,* Wiley, New York, 1983, pp. 147–180.

[22]Carlson, G. E., and Halijak, C. A., "Approximation of Fractional Capacitors $(1/s)^{1/n}$ by a Regular Newton Process," *IEEE Transactions on Circuit Theory,* June 1964, pp. 210–213.

[23]Miller, D. W., and Crawley, E. F., "Experimental Investigations into Passive and Active Control Using Space-Realizable Techniques," *Journal of Guidance, Control, and Dynamics,* Vol. 11, No. 5, 1988, pp. 449–458.